Pharmacological Targeting of Androgen Receptor Elicits Context-Specific Effects in Estrogen Receptor–Positive Breast Cancer

Lixuan Wei[1], Huanyao Gao[1], Jia Yu[1], Huan Zhang[1], Thanh Thanh L. Nguyen[1], Yayun Gu[1], Marie R. Passow[2], Jodi M. Carter[2], Bo Qin[1,3], Judy C. Boughey[4], Matthew P. Goetz[1,3], Richard M. Weinshilboum[1], James N. Ingle[3], and Liewei Wang[1]

ABSTRACT

Androgen receptor (AR) is expressed in 80% to 90% of estrogen receptor α–positive (ER^+) breast cancers. Accumulated evidence has shown that AR is a tumor suppressor and that its expression is associated with improved prognosis in ER^+ breast cancer. However, both a selective AR agonist (RAD140) and an AR inhibitor (enzalutamide, ENZ) have shown a therapeutic effect on ER^+ breast cancer, so the potential for clinical application of AR-targeting therapy for ER^+ breast cancer is still in dispute. In this study, we evaluated the efficacy of ENZ and RAD140 *in vivo* and *in vitro* in AR^+/ER^+ breast cancer models, characterizing the relationship of AR and ER levels to response to AR-targeting drugs and investigating the alterations of global gene expression and chromatin binding of AR and ERα after ENZ treatment. In the AR-low setting, ENZ directly functioned as an ERα antagonist. Cell growth inhibition by ENZ in breast cancer with low AR expression was independent of AR and instead dependent on ER. In AR-high breast cancer models, AR repressed ERα signaling and ENZ promoted ERα signaling by antagonizing AR. In contrast, RAD140 activated AR signaling and suppressed AR-high tumor growth by deregulating ERα expression and blocking ERα function. Overall, analysis of the dynamic efficacies and outcomes of AR agonist, and antagonist in the presence of different AR and ERα levels reveals regulators of response and supports the clinical investigation of ENZ in selected ER^+ tumors with a low AR/ER ratio and AR agonists in tumors with a high AR/ER ratio.

Significance: The ratio of androgen receptor to estrogen receptor in breast cancer dictates the response to AR-targeted therapies, providing guidelines for developing AR-directed treatment strategies for patients with breast cancer.

Introduction

Breast cancer is the most commonly diagnosed malignancy among women with an estimated 2.3 million new cases in 2020 worldwide (1). Despite advances in detection and treatment, this disease remains one of the leading causes of cancer-related mortality (2, 3). Over 70% of breast cancers express estrogen receptor α (ERα), which is an estrogen-activated transcription factor that drives tumor growth and progression (4, 5). Estrogen suppression and ER blockade are the main approaches used to treat ER^+ breast cancer. Approved adjuvant endocrine therapies for ER^+ breast cancer include selective ER modulators and aromatase inhibitors (AI; ref. 6). In early-stage breast cancers, endocrine therapies have considerably decreased cancer recurrence and mortality (7, 8). However, about 20% of ER^+ patients recur with metastatic disease after 5 years of adjuvant endocrine therapy (8). Thus, more durable and effective therapeutics are needed to decrease recurrences in early-stage breast cancer.

The androgen receptor (AR) is expressed in 80% to 90% of ER^+ breast cancer (4, 5, 9) and higher expression of AR is associated with improved overall survival (OS) and disease-free survival (DFS; refs. 5, 9–11). The role of AR in the context of ER^+ breast cancer has long been a disputed issue. Some researchers claimed that AR is an oncogenic protein. They found that the native ligand of AR (5α-dihydrotestosterone, DHT) stimulated ER^+ breast cancer growth (12, 13). DHT was also reported to promote ER^+ breast cancer metastasis by epigenetically upregulating E-cadherin and vimentin expression (14). A recent clinical trial with enzalutamide, the AR blocker in ER^+ also showed the potential benefits of ENZ in a subpopulation (15). AR degrader was effective in repressing the growth of ER^+ breast cancer cell lines (16). However, accumulating evidence has shown that AR is a tumor suppressor in ER^+ breast cancer. Androgens showed a tumor suppression effect (17) and were used to treat breast cancers in the 20th century (18, 19). The treatment with androgen inhibits cellular proliferation in different ways. It can interfere with ER-dependent transcription by competing for the binding to the same sites or facilitating the ER binding to the DNA (20). Shared coactivators might also be involved in the ERα transcriptional interference caused by AR overexpression (21). In addition, AR activation induced ER beta upregulation and miR-21 downregulation that contribute to the protective effect of AR (22). Specifically, a recent study revealed the tumor suppressor role of AR (23). The genomic distribution of ER and essential coactivators (p300, SRC-3) was altered by AR activation, resulting in the repression of ER-regulated cell-cycle genes and upregulation of AR target genes. More interestingly, some studies indicate that AR is responsible for metastasis and endocrine resistance in ER^+ breast cancer. AR expression levels

[1]Department of Molecular Pharmacology and Experimental Therapeutics, Mayo Clinic, Rochester, Minnesota. [2]Department of Laboratory Medicine and Pathology, Mayo Clinic, Rochester, Minnesota. [3]Department of Oncology, Mayo Clinic, Rochester, Minnesota. [4]Department of Surgery, Mayo Clinic, Rochester, Minnesota.

Corresponding Author: Liewei Wang, Mayo Clinic, 200 First Street Southwest, Rochester, MN 55905. Phone: 507-284-5264; Fax: 507-284-4455; E-mail: Wang.Liewei@mayo.edu

Cancer Res 2023;83:456–70

doi: 10.1158/0008-5472.CAN-22-1016

are elevated in bone biopsies of metastatic breast cancer and are correlated with the duration of treatment with AIs (24). AR overexpression induces tamoxifen and anastrozole resistance in breast cancer cells (25, 26). These findings provide a rationale for targeting AR in patients with both early-stage breast cancer and endocrine-resistant breast cancer.

Although both AR agonists and antagonists have shown a therapeutic effect on ER$^+$ breast cancer, it is unclear which tumor profile might benefit from stimulating AR versus inhibiting AR. Enzalutamide (ENZ), an AR antagonist, impairs AR signaling, inhibits ER$^+$/AR$^+$ breast cancer cell proliferation, and restores the sensitivity of antiestrogen therapies (27, 28). The *in vivo* or clinical efficacy of ENZ is not established. ENZ inhibited estrogen-stimulated growth of MCF7 and PT12 xenograft tumors and showed repressing effects on the growth of tamoxifen-resistant MCF7 xenografts (27, 28). However, ENZ did not affect the growth of ZR75–1 xenografts (23) or endocrine-resistant patient-derived xenografts (PDX; ref. 29). The combination of ENZ and exemestane did not show an improved progression-free survival (PFS) compared with exemestane alone, although it showed a potential benefit in a subpopulation (15). As mentioned previously, the effect of AR agonists on ER$^+$ breast cancer proliferation is controversial. Recently, selective AR modulators (SARM) RAD140 and enobosarm showed potential clinical benefits on ER$^+$ breast cancer (23, 30). RAD140 suppressed the growth of ER$^+$/AR$^+$ breast cancer by stimulating AR signaling, resulting in the downregulation of ERα (30). DHT inhibited estrogen-regulated gene expression, epithelial–mesenchymal transition (EMT), and distant metastasis in ESR1-mutant tumors (31). These divergent results have significantly confounded the implementation of AR-targeting therapies. The therapeutic efficacy of AR agonists and AR antagonists needs clarification to better characterize their clinical application. Therefore, we investigated ENZ and RAD140 response in multiple ER$^+$ breast cancer cells and PDX models and demonstrated the gene expression and genomic-binding alterations after drug treatment. Our results support the clinical trials of ENZ, an AR antagonist, in selected ER$^+$ tumors with a low AR/ER ratio and RAD140, an AR agonist, in tumors with a high AR/ER ratio.

Materials and Methods

Cell lines, plasmids, and reagents

Human breast cancer cell lines were purchased from the ATCC (breast cancer cell panel, 30–4500KTM). All cell lines were characterized by STR analysis and tested for free from *Mycoplasma* infection (IDEXX Laboratories). T47D (CVCL_0553) and HCC1419 (CVCL_1251) cells were maintained in RPMI-1640 medium with 10% FBS. MCF7 (CVCL_0031), CAMA1 (CVCL_1115), and HEK293T (CVCL_0063) cells were maintained in EMEM medium with 10% FBS. MCF10A (CVCL_0598) was obtained from the ATCC and maintained following its instruction. All cells were grown in an atmosphere of 5% CO_2 and 37°C. Cells used in all experiments were below 10 passages. Compounds used in this study were purchased from Selleckchem (ENZ, S1205; RAD140, S5275; Apalutamide, S2840; Darolutamide, S7559), Cayman Chemical (RD162, 13039) and Sigma (E2, E2758, DHT, D073). Doxycycline was ordered from Takara (631311).

Human AR full-length was cloned into the PCMV6-XL4 vector (Origene), pLVX-Puro vector (Takara Bio), and the Lenti-X Tet-One Inducible vector (Takara Bio). Human ESR1 was cloned into the PCMV6-XL4 vector and Lenti-X Tet-One Inducible vector. ESR1 shRNAs were cloned into pLKO.1 vector (Sigma). Human AR was knocked out using Edit-R CRISPR-Cas9 gene engineering with Cas9 nuclease expression plasmids (Cat. #U-005100–120), synthetic CRISPR RNA (crRNA), and transactivating CRISPR RNA (tracrRNA) system (Dharmacon). The target sequences of shRNA, siRNA, and crRNA are listed in Supplementary Table S1.

Stable cell–line generation

Lentivirus plasmids were packaged using a VSV-G lentiviral packaging kit (631275, Takara). Packaged lentivirus was produced in HEK293T cells. MCF7 and T47D cells were infected with the indicated lentivirus in the presence of 10 μg/mL polybrene. Transduced MCF7 and T47D cells were cultured for 2 days. Positive cells were selected using puromycin at 1 μg/mL for 2 weeks. Single cells were picked and cultured in complete media for 1 to 2 months. Isolated clones were analyzed using immunoblot and qRT-PCR. For AR gene knockout, MCF7 and T47D cells were transfected with Cas9 nuclease expression plasmid and selected with puromycin for 1 week. The mixture of three crRNA-targeting AR and tracrRNA was cotransfected to Cas9-positive cells. Cells were seeded at 100 cells per 96-well plates. Single clones were tested using Western blot.

Cell proliferation and colony formation assays

For proliferation assays, cells were seeded in medium with 10% CSS at 2,000 cells per well in 96-well plates and subjected to treatment with ENZ, RAD140, DHT, or DMSO for 5 or 12 days with treatments being renewed every 3 days. Cell viability was measured using the CyQUANT Kit (C7026, Thermo Fisher Scientific). Each experiment having three replicates was performed three times. For the colony formation assay, 500 cells were seeded in duplicate in 6-well plates and allowed to grow until visible colonies formed in complete growth media or steroid-stripped media (3–6 weeks). For treatments, ENZ, RAD140, DHT, or DMSO were added the following day after seeding the cells and were renewed every 3 days.

qRT-PCR and Western blot analysis

Total RNA was extracted from cell lines or frozen tumor tissues using the RNA isolation kit (74134, Qiagen). One-step qRT-PCR was performed in triplicate using the SYBR Green method (4389986, Thermo Fisher Scientific) on QuantStudio real-time PCR system (Thermo Fisher Scientific) with the primers (Supplementary Table S1). The measurement of individual RNA expression was determined relative to the levels of *GAPDH* transcript. Protein extracts from cells were prepared using RIPA lysis buffer. Nuclear and cytoplasmic proteins were isolated using NE-PER Nuclear and Cytoplasmic Extraction Reagents (78833, Thermo Fisher Scientific). Cell lysate concentration was measured by Protein Assay Dye (Bio-Rad). Proteins were resolved in SDS-PAGE followed by immunoblotting analysis. The antibodies used are listed in Supplementary Table S2. The intensity of the band was quantified using ImageJ software (https://imagej.nih.gov/ij/).

ERE luciferase assay

Transcription activity of ERα was measured using the dual luciferase assay with the Cignal ERE Reporter Assay Kit (Qiagen). AR CRISPR knockout and control T47D cells were cultured in charcoal-stripped serum medium for 48 hours and then switched to serum-free medium in 48-well plates for 1 day. Cells were then transfected with ERE reporter constructs using the Lipofectamine 2000 transfection reagent. After 24 hours of transfection, cells were treated with E2, ENZ, or E2 plus ENZ for 24 hours. Luciferase was tested using the Dual-Luciferase Reporter Assay System from Promega following the manufacturer's protocol.

Radiolabeled ligand receptor–binding assay

Recombinant full-length human AR and ERα protein ordered from Creative Biomart. [3H]-ENZ and [3H]-17β-estradiol were synthesized by PerkinElmer. Assay buffer (10 mmol/L Tris-HCl; 1 mmol/L EDTA; 1 mmol/L EGTA; 1 mmol/L NaVO3; 1% glycerol; 0.25 mmol/L leupeptin; 1% BSA; 1 mmol/L DTT) was prepared one week before experiments. ERα saturation–binding assays were performed to measure total binding and nonspecific binding (NSB). 1 nmol/L ERα was incubated with radioactive ENZ (1–500 nmol/L) overnight at 4°C. To determine NSB, a 100-fold excess of cold ENZ was added and incubated together. AR saturation–binding assay using 0.5 to 25 nmol/L hot ENZ, 1,000× cold compound, and 100 nmol/L AR protein in the reaction. Bound and unbound ligands were separated by incubation with ice-cold dextran-coated charcoal on ice for 10 minutes. The radioactivity of bound ligands was then measured using a Beckmann LS 6500 liquid scintillation counter (Ramsey). The equilibrium dissociation constant for the radioligand (K_D) was calculated using non-linear regression analysis. [3H]-17β- estradiol displacement assays were performed in the same condition using 1 nmol/L hot estradiol and increasing concentrations of nonradioactive ligand, for example, cold estradiol (10 nmol/L–100 μmol/L) or ENZ (1–200 μmol/L). Competition curves were plotted as the percentage of hot estradiol-binding versus increasing concentrations of unlabeled ligands.

RNA sequencing

MCF7-Tet cells were used to create AR-low (no doxycycline) and AR-high cells (doxycycline 800 ng/mL). Doxycycline was added to cell culture media 1 day before drug treatments. MCF7 parental and AROE cells were treated with DMSO or Enzalutamide (10 μmol/L) for 24 hours. One control sample and duplicate samples under ENZ treatment were collected for RNA sequencing. Total RNA was extracted using the RNeasy Plus Mini kit (74134, Qiagen) per the manufacturer's instructions. Poly-A enriched RNA library prep and sequencing were done by Mayo Next Gen sequencing cores using Illumina truseq2 kit. Individual libraries were pooled and run on HiSeq 4000 system (2×150 paired-end, Illumina). Filtered reads were aligned to the hg38 human reference genome using STAR with an average mapping rate of 93%. Raw counts were then called by HTSeq excluding non-unique mapped reads. Differential expression analysis was performed by EdgeR package using R software. Upstream analysis was done in Ingenuity Pathway Analysis (IPA) software (32). Gene set enrichment and pathway analyses were implemented using the Broad Institute's public server (https://www.gsea-msigdb.org/gsea/index.jsp) with default parameters.

AR and ERα ChIP sequencing

AR expression was induced by doxycycline (800 ng/mL) for 24 hours in MCF7-Tet cells. Cells were treated with DMSO or ENZ (10 μmol/L) for 2 hours. 1×10^8 cells were fixed in 1% formaldehyde for 20 minutes at room temperature and 0.1 volume of 2 mol/L glycine was added to quench the reaction. Cell lysis was sonicated to fragment chromatin to 200–300 bp. Solubilized chromatin was subjected to immunoprecipitation with the AR and ERα antibodies (Supplementary Table S2). Library prep and sequencing were done in the Epigenomics Development Laboratory of Mayo Clinic. Libraries were sequenced using 100-bp paired-end reads on the Illumina platform at the Mayo Clinic.

Sequence alignment and peak calling were done by the Bioinformatics core at Mayo Clinic. Sequences were aligned to the Human Reference Genome (assembly hg38, UCSC, December, 2013) using BWA version 0.7.17. Enriched regions of the genome were identified by comparing the chromatin immunoprecipitation (ChIP) samples to input samples using the MACS2 peak caller version 2.1($P_{adj} < 0.01$). After identifying a common set of peaks, peaks overlapping were analyzed using the ChIPpeakAnno package in R (max peak gap, 1kb). The motif enrichment was tested using the HOCOMOCO database and was done in the MEME suite (https://meme-suite.org/meme/doc/meme-chip.html). The heat maps of the raw ChIP-seq data were generated using deepTools 2.0 (https://deeptools.readthedocs.io/en/develop/). The peaks around certain genes were displayed in WashU Epigenome Browser (https://epigenomegateway.wustl.edu/).

Animal models and treatment approach

Animal experiments using MCF7 cell-line and PDX models were performed at the Mayo Clinic under Institutional Animal Care and Use Committee approval (Protocol ID: A00005364–20). Six- to 8-week-old female NOD.Cg-Prkdc^{scid} Il2rg^{tm1Wjl}/SzJ mice were used in all animal models (IMSR_JAX:005557, The Jackson Laboratory). These xenograft models were supplemented with exogenous estradiol in drinking water (8 mg/mL, 2/wk refreshed). Ten-million cells were suspended in 100 μL Matrigel and injected into the mammary fat pad to generate cell-line xenografts. The ER$^+$ breast cancer PDX models were established by implanting tumor fragments subcutaneously in the flank of female mice. The cell-line or PDXs with volumes between 100 and 200 mm^3 were enrolled in treatment groups. Enzalutamide or RAD140 was administered as a single agent or in combination with fulvestrant. ENZ (25 mg kg^{-1} d^{-1}) and RAD140 (50 mg kg^{-1} d^{-1}) were resuspended in 0.5% carboxymethyl cellulose and delivered 5 times per week by oral gavage. Fulvestrant was given as subcutaneous injection (2 mg/wk in sesame oil). Tumor volume and body weight were measured twice a week. Tumor volume was calculated using the formula (length × width^2) / 2. Upon reaching experimental endpoints, mice were sacrificed and the primary tumors were kept at −80°C for further analysis.

IHC analysis

MCF7 and MCF7 AROE xenograft tumors were removed and fixed in neutral buffered 10% formalin at room temperature for 24 hours before embedding in paraffin and sectioning. Sections were prepared at the Animal Histology Core Laboratory of Mayo Clinic. Tissue sections of MCF7 and MCF7 AROE xenografts were deparaffinized and then subjected to AR, ERα, and Ki67 immunochemistry according to the manufacturer's instructions diaminobenzidine (DAB 150, Millipore). Stable DAB was used as a chromogenic substrate, and the sections were counterstained with a hematoxylin solution. Photographs of the entire cross-section were digitized using Aperio AT2 slide scanner (Leica).

Breast cancer tissue microarray (TMA) was purchased from US Biomax (BR2089). AR and ER IHC were performed in the CAP/CLIA-certified Clinical IHC laboratory (Mayo Clinic) using Ventana Medical Systems (Roche). The antibodies used were listed in Supplementary Table S2. In each tissue core, the percentage of AR or ER-immunoreactive invasive tumor nuclei per total evaluable invasive tumor nuclei was scored manually in decile increments (0%–100%). The average staining intensity of the immunoreactive nuclei was assessed semiquantitatively on a scale of 0 to 3 (none, weak, intermediate, and strong). The percentage equals the percentage of tumor nuclei staining. The expression levels were scored by multiplying the percentage of positive cells by the intensity.

Statistical analyses

Statistical calculations were performed using GraphPad Prism (GraphPad Software) and R 4.1.2 software. *In vitro* proliferation and colony formation experiments were analyzed by two-tailed Student *t* test. Tumor growth curve data were analyzed at an ethical endpoint using a two-tailed, unpaired Student *t* test. mRNA expression of xenografts and mice weight in the different treatment groups were compared using two-tailed, unpaired Student *t* test. Linear regression was used to test the association between the dose-response AUC and AR, ER, or AR/ER levels. Two-tailed Spearman's correlation test was used to analyze the relationship between AR and ERα expression. Two-tailed, unpaired Student *t* test was used to test the difference between AR, ER, or AR/ER levels in primary and metastatic breast cancer. Survival curves were plotted by the Kaplan–Meier method and compared using the log-rank test. If not stated otherwise, all values represent means of at least three independent experiments ± SD. $P < 0.05$ was considered statistically significant (*, $P < 0.05$; **, $P < 0.01$; ***, $P < 0.001$).

Data availability

The RNA-seq and ChIP-seq data reported in this study are available from Gene Expression Omnibus (GEO, GSE200300 ChIP-seq, GSE200435 RNA-seq). All other data are available from the corresponding author (Liewei Wang, Wang.Liewei@mayo.edu) upon reasonable request.

Results

Differential response to AR agonist and antagonist in ER$^+$ breast cancer cell lines

To investigate the antitumor efficacy of AR-targeting therapy and mechanisms underlying conflicting results with the application of AR agonists versus antagonists, we first tested the cell growth inhibition rate of the AR agonist (DHT) and the AR antagonist (ENZ) using ER$^+$ cell lines. We measured AR and ER levels in ER$^+$ cell lines and found that HCC1419 and CAMA1 have relatively higher AR expressed than T47D and MCF7 (Supplementary Fig. S1A). In MCF7 and T47D cells, with relatively low AR expressed, ENZ substantially inhibited cell growth but DHT, within the normal physiological range (33), had no effects on cell growth compared with DMSO treatment (**Fig. 1A** and **B**; Supplementary Fig. S1B and S1C). Alternatively, in HCC1419 and CAMA1 cells, we observed a significant reduction of cell growth after DHT treatment but no change with ENZ treatment (**Fig. 1C** and **D** and Supplementary Fig. S1D and S1E). In addition, we found that DHT decreased cell growth rates when its target, AR, was overexpressed in MCF7 and T47D cells (Supplementary Fig. S1F–S1H). RAD140, a breast tissue-selective AR agonist (30), also showed growth inhibition effects in cells with high AR. In contrast with RAD140, ENZ impaired cell proliferation only in MCF7 and T47D cells. Surprisingly, ENZ even promoted cell growth in CAMA1 cells (**Fig. 1E**–**H**). To further confirm the drug–response profile in two subgroups of cells, we generated stable AR-overexpressed MCF7 cells, picked 3 single clones with different AR expression levels (**Fig. 1I**), and assessed the antiproliferation activity of drugs in control and AR-overexpressed cells. As we expected, the AR agonist RAD140 inhibited cell growth when AR was much higher expressed than control cells (AR-PLVX3#2 and AR-PLVX3#3 vs. PLVX3). Meanwhile, those AR-overexpression cells became more resistant to ENZ (**Fig. 1J**). We also knocked down AR in HCC1419, a high AR cell, and tested the response of ENZ and RAD140. We found that AR-knockdown (KD) cells were more sensitive to ENZ than parental cells (Supplementary Fig. S1I and S1J). The cell growth inhibition effect of RAD140 was impaired when AR was knocked down (Supplementary Fig. S1K). It has been reported recently that AR is a tumor suppressor in ER$^+$ breast cancer and an AR agonist can be used to treat ER$^+$ breast cancer (23). In our experiments, we found that the AR agonist only inhibited AR "high" breast cancer cells and ENZ had a better growth inhibition effect in AR "low" cells, suggesting that the efficacy of AR-targeting drugs largely depended on the context of AR and ERα status.

The cell growth inhibition of enzalutamide in "AR-low" breast cancer is not dependent on AR but rather on ER

The observation that ENZ had better inhibition in AR-low cells prompted us to hypothesize that ENZ might not target its canonical target AR in these cells. We generated AR knockout (ARKO) MCF7 and T47D cells using the CRISPR/cas9 system and tested ENZ response in control and ARKO cells. Results showed that the cell growth inhibition effect of ENZ was not significantly impaired when the AR was knocked out, indicating that ENZ might have non-canonical targets in cells lacking the AR (**Fig. 2A**–**D**). To further understand the mechanism of ENZ underlying the observation in the two groups of breast cancer cells selected on the basis of AR levels, we created Tet-induced AR-overexpression MCF7 cells (Supplementary Fig. S2A) and performed RNA sequencing with DMSO or ENZ treatment in both control cells and AR overexpression cells. We identified 193 differential expressed genes (76 up and 117 down) between DMSO and ENZ-treated parental MCF7 cells (FC>2 or <0.5, FDR<0.05, Supplementary Table S3). To determine the pathways targeted by ENZ in parental MCF7 cells where we saw a cell growth inhibition, we did the upstream analysis with the 193 ENZ-affected genes in MCF7 cells using IPA software (32). The results showed that ER might be the upstream regulator of those differentially expressed genes regulated by ENZ and ER signaling was predicted to be inhibited after ENZ treatment ($P = 1.69\times10^{-10}$, **Fig. 2E**). We performed global ERα ChIP-seq in MCF7 parental cells incubated with DMSO or ENZ and found that 39.58% (8,681/21,933) of ER-bound sites were abolished by ENZ (**Fig. 2F**, Lost ERBS) and the binding intensity was significantly decreased upon ENZ treatment in 12,868 conserved ER-binding sites (**Fig. 2F** and **G**). We observed a significantly decreased effect of ENZ on colony formation in ER knockdown (ERKD) cells compared with control cells (**Fig. 2H** and **I**; Supplementary Fig. S2B). This observation suggests that ENZ inhibits cell growth in AR-low ER$^+$ cells by decreasing ERα genomic binding and blocking ERα signaling in hormone-replete conditions, which is consistent with previously published reports that ENZ reduced estradiol (E2)–mediated proliferation and genomic ERα binding in MCF7 cells (27).

To determine how ENZ inhibited ER activity, we first tested AR and ERα expression levels with ENZ treatment in MCF7 and T47D cells. 10 μmol/L ENZ caused 12% and 25% decrease in ERα levels compared with DMSO in MCF7 and T47D cells, respectively (Supplementary Fig. S2C). Both cytosolic and nuclear ERα were downregulated after ENZ treatment in T47D cells (Supplementary Fig. S2D). ENZ can directly bind to AR and impair AR downstream signaling (34), which led us to compare the binding affinity of ENZ with AR and ERα. We performed radiolabeled-binding assays to measure the binding affinity of ENZ with ERα and AR. Results showed that ENZ directly bound to ERα with a $K_D = 399.60$ nmol/L, whereas much higher affinity was shown for AR ($K_D = 24.13$ nmol/L; **Fig. 2J**; Supplementary Fig. S2E). Moreover, ENZ acted as an ERα antagonist and partially competed with E2 for ERα binding (**Fig. 2K**). The estrogen response element (ERE) luciferase assay showed that E2-induced ER activity was blocked in both parental and ARKO T47D

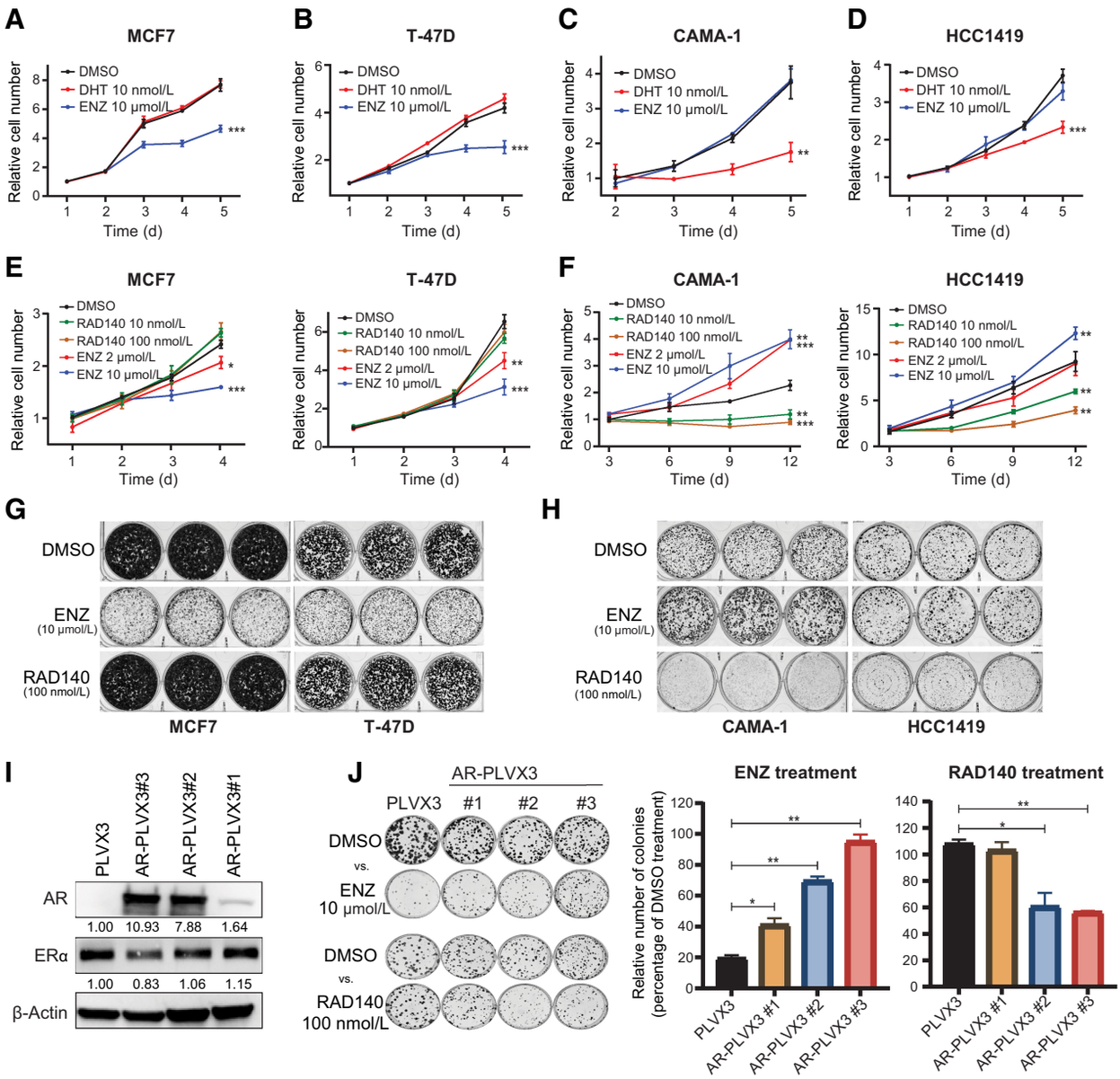

Figure 1.

The response of AR agonist and antagonist in ER$^+$ breast cancer cell lines. **A–F,** Relative numbers of cells grown in the presence of DMSO, DHT, ENZ, and RAD140. **A, B,** and **E,** AR antagonist ENZ inhibited cell growth and AR agonist DHT or RAD140 did not affect cell proliferation in MCF7 and T47D cells. **C, D,** and **F,** AR agonist DHT or RAD140 decreased cell growth. Long time (>9 days) AR antagonist exposure promoted cell growth in CAMA1 and HCC1419 cells. **G** and **H,** Colony formation assays with DMSO, ENZ, or RAD140 treatment in four cell lines. **G,** MCF7 and T47D cells. **H,** CAMA1 and HCC1419 cells. Cell colonies were markedly reduced by ENZ in MCF7 and T47D cells. RAD140 impaired cell colony formation in CAMA1 and HCC1419 cells. **I,** Immunoblot analysis of MCF7 stable cell lines expressing control vector (PLVX3) and AR (AR-PLVX3). Relative AR protein levels were quantified using ImageJ software. **J,** Representative images and quantification of colony formation assays in MCF7 control and AR overexpression cells with DMSO, ENZ, or RAD140 treatment. ENZ effects were tested in complete media. RAD140 treatment was performed in the hormone-depleted medium. For proliferation assays, compared relative cell numbers in DMSO and drug treatments on the last day of observation (4, 5, or 12 days). In cell colony quantification, comparisons were performed between AR-PLVX3 and PLVX3. All error bars represent SD. Two-tailed Student *t* test, *, $P < 0.05$; **, $P < 0.01$; ***, $P < 0.001$.

cells (Supplementary Fig. S2F). We also observed an inhibition effect of ENZ in ER overexpressed MCF10A cells that had limited AR and ER expression (Supplementary Fig. S2G). These data indicated that ENZ blocked ERα activity in cells with low AR by directly functioning as an ER antagonist.

To determine whether the different effects in AR-low or -high cells are common among AR antagonists, we tested the efficacy of three other AR antagonists (RD162, apalutamide, and darolutamide) in AR-high and -low cells. The molecular structure of RD162 and apalutamide is closely related to ENZ (34, 35), whereas darolutamide

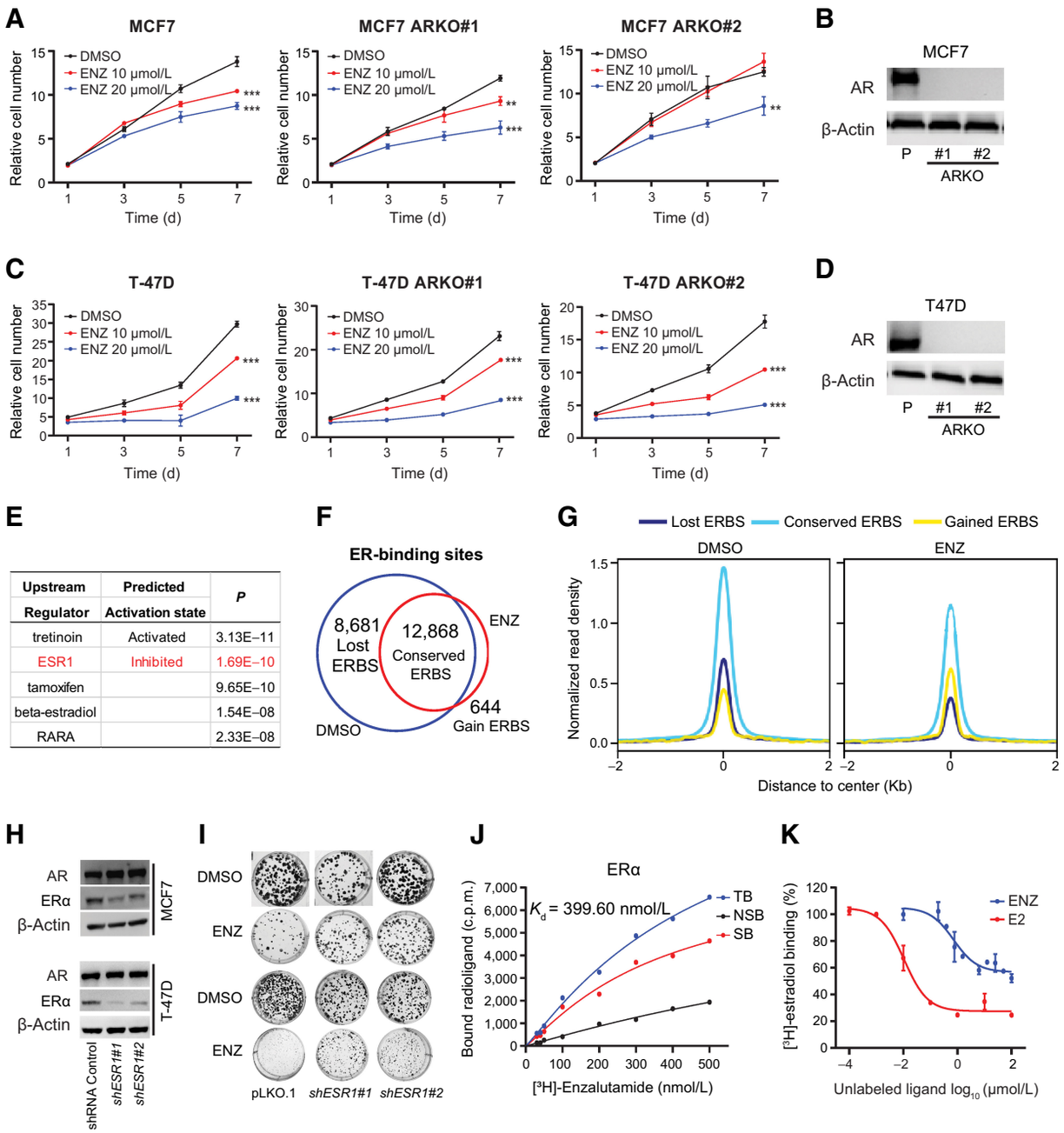

Figure 2.

ENZ antagonized ERα activity in cells with low abundance of AR. **A,** Cell growth curves under DMSO and 10 and 20 μmol/L ENZ treatment of parental and AR knockout MCF7 cells. Two signal colonies of knockout cells were chosen. **B,** Western blot showing AR expression in parental and AR knockout MCF7 cells. **C,** Cell growth curves under DMSO and 10 and 20 μmol/L ENZ treatment of parental and AR knockout T47D cells. Two signal colonies of knockout cells were chosen. **D,** Western blot showing AR expression in parental and AR knockout T47D cells. **E,** Upstream regulators of ENZ-affected genes. The 193 differentially expressed genes after ENZ treatment (FC > 2 or < 0.5, FDR < 0.05) were identified by RNA sequencing of MCF7 cells treated with DMSO or 10 μmol/L ENZ for 24 hours. Upstream stream analysis was done in Ingenuity Pathway Analysis software. **F,** Overlap of ER cistrome under DMSO and 10 μmol/L ENZ treatment in MCF7 cells. **G,** Histogram plot of average read density around lost (dark blue), gained (yellow), and conserved (light blue) ER-binding sites (ERBS) in MCF7 cells with DMSO or ENZ treatment. **H,** Western blot showing AR and ER expression in MCF7 and T47D cells stably expressed shRNA control, *shESR1#1* and *shESR1#2*. **I,** Colony formation assays with DMSO or ENZ treatment in control and ER stable knockdown cells. DMSO or 10 μmol/L ENZ was added to cell culture media for 3 weeks. **J,** Saturation-binding curve of [^{3}H]-ENZ to ER. TB, total binding; NSB, nonspecific binding; SB, specific binding; K_d, equilibrium dissociation constant. SB was calculated by subtracting NSB from TB. **K,** [^{3}H]-estradiol competition-binding curves. Data are expressed as percentages of specific binding of [^{3}H]-estradiol versus log of the competitor concentration (cold E2 concentrations ranged from 1 nmol/L to 100 μmol/L; concentrations of ENZ ranged from 0.1 to 100 μmol/L). Each point represents the mean ± SD of three independent determinations. Relative cell numbers under DMSO and drug treatments on the last day of observation were compared in the proliferation assays. All error bars represent SD. Two-tailed Student *t* test, **, $P < 0.01$; ***, $P < 0.001$.

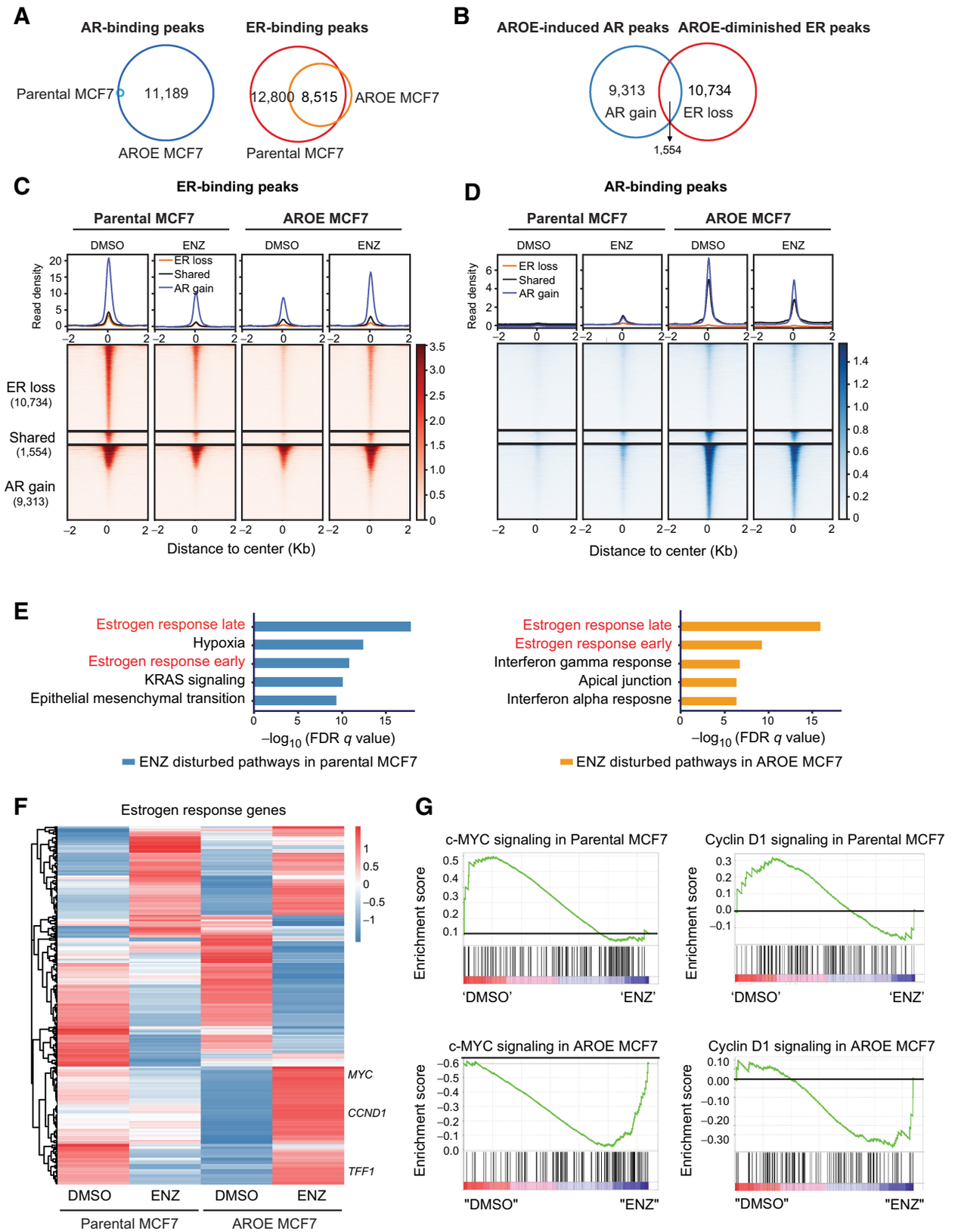
A
AR-binding peaks
ER-binding peaks
Parental MCF7
11,189
AROE MCF7
12,800
8,515
AROE MCF7
Parental MCF7
B
AROE-induced AR peaks
AROE-diminished ER peaks
9,313
AR gain
10,734
ER loss
1,554
C
ER-binding peaks
Parental MCF7
AROE MCF7
DMSO
ENZ
DMSO
ENZ
Read density
ER loss
Shared
AR gain
ER loss
(10,734)
Shared
(1,554)
AR gain
(9,313)
Distance to center (Kb)
D
AR-binding peaks
Parental MCF7
AROE MCF7
DMSO
ENZ
DMSO
ENZ
Read density
ER loss
Shared
AR gain
Distance to center (Kb)
E
Estrogen response late
Hypoxia
Estrogen response early
KRAS signaling
Epithelial mesenchymal transition
–log10 (FDR q value)
ENZ disturbed pathways in parental MCF7
Estrogen response late
Estrogen response early
Interferon gamma response
Apical junction
Interferon alpha resposne
–log10 (FDR q value)
ENZ disturbed pathways in AROE MCF7
F
Estrogen response genes
MYC
CCND1
TFF1
DMSO
ENZ
DMSO
ENZ
Parental MCF7
AROE MCF7
G
c-MYC signaling in Parental MCF7
Cyclin D1 signaling in Parental MCF7
Enrichment score
'DMSO'
'ENZ'
c-MYC signaling in AROE MCF7
Cyclin D1 signaling in AROE MCF7
Enrichment score
"DMSO"
"ENZ"

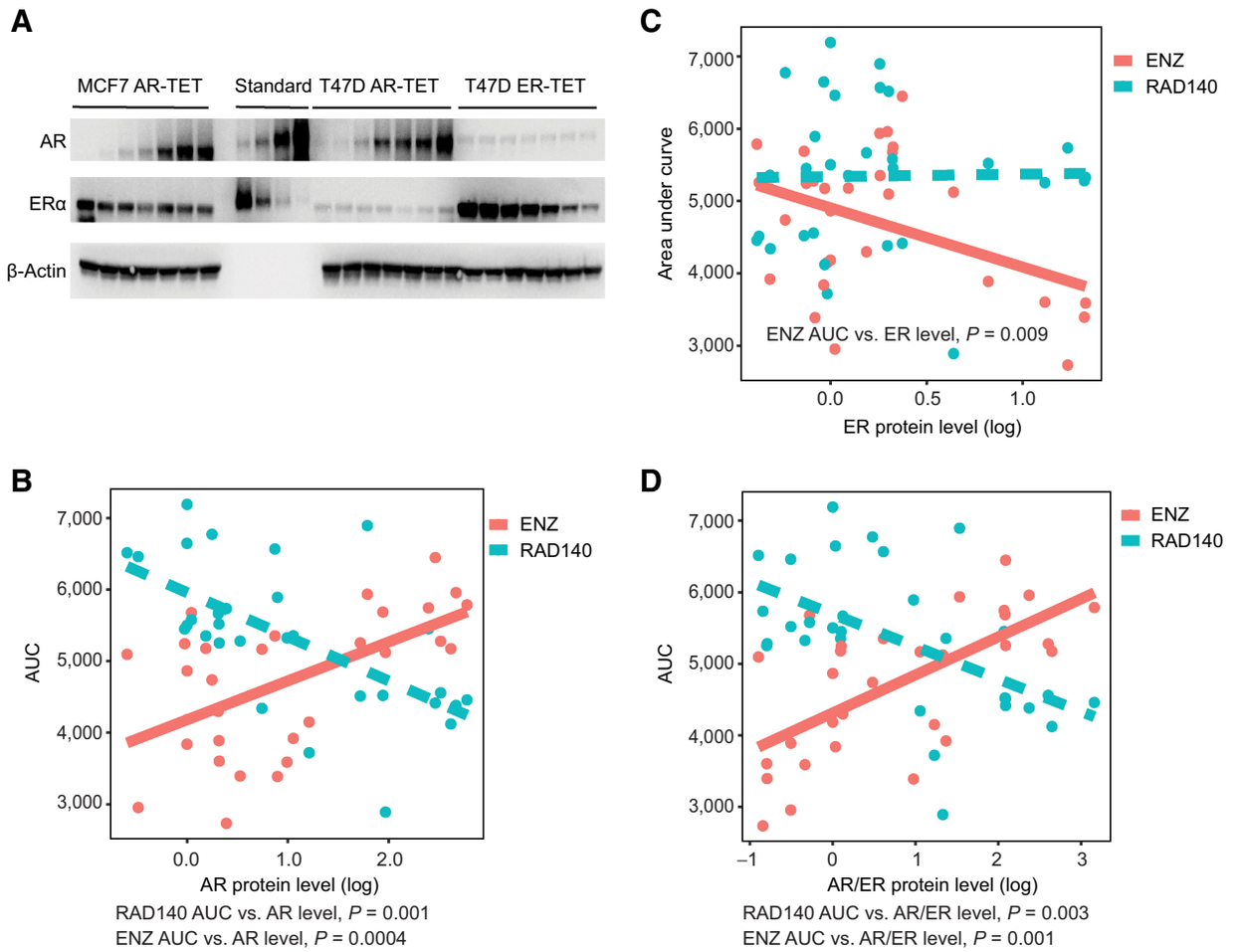

Figure 4.

The association between AR/ER and the response to ENZ and RAD140. **A,** AR and ER expressions in Tet-inducible MCF7 and T47D cells. AR or ER was induced by doxycycline (0–800 ng/mL). Band intensities were quantified by ImageJ and normalized to vehicle treatment of each cell line. **B–D,** Cytotoxicity curves of cells with a series of AR, ER, and AR/ER levels were plotted after 5 days of incubation of ENZ (0.78–100 μmol/L) or RAD140 (0.1 nmol/L–100 μmol/L). The area under cytotoxicity curves (AUC) was calculated using a fitted dose–response curve by the AUC function from DescTool package. Relationship between AUC and $\log_2$(AR), $\log_2$(ER) level, or $\log_2$(AR/ER) ratio was modeled by linear regression. *P* values represent test for the significance of the fitted slope parameter. **B** and **C,** Both AR and ER levels are associated with ENZ response. Higher ER and lower AR are related to better response to ENZ than lower ER and higher AR. Higher AR is associated with a better response to RAD140 than lower AR. **D,** The AR/ER ratios were significantly positively associated with the AUC of ENZ and negatively associated with the AUC of RAD140.

Figure 3.

ENZ reclaims AR-mediated repression of ER signaling. **A,** Venn diagram demonstrates the differences in ER- and AR-binding sites performed on MCF7 parental and AROE cells. AR-high (overexpression, OE) cells were created by doxycycline induction for 24 hours. Compared with MCF7 cells, 11,189 AR-binding peaks were newly detected (induced AR peaks) and 12,800 ER-binding peaks disappeared (diminished ER peaks) in AROE cells. **B,** Venn diagram demonstrates the overlap between induced AR peaks and diminished ER peaks. After AR OE, 9,313 peaks gained AR binding, 10,734 peaks lost ER binding, and 1,554 peaks had both AR gain and ER loss at the same sites. **C** and **D,** Read density plot (top) and heatmap (bottom) of ER (**C**) and AR (**D**) ChIP-seq data derived from MCF7 parental and AROE cells treated for 4 hours with DMSO or ENZ (10 μmol/L). Read density plot and heatmap depict the binding intensity around ER loss, AR gain, and shared (both AR gain and ER loss) peaks under DMSO and ENZ treatment in a ±2Kb genomic window. **E,** Pathway analysis of ENZ-induced genes in parental and AROE MCF7 cells. Differentially expressed genes (FC > 1.5 or <0.67, FDR < 0.05) were used to run hallmark gene sets enrichment in GSEA websites. **F,** Heatmap displays the expression of estrogen response genes following 24 hours of DMSO and ENZ treatment in parental and AROE MCF7 cells. **G,** Gene set enrichment plots for oncogenic signature gene sets found the opposite effect of ENZ in parental and AROE MCF7 cells. ENZ downregulated c-MYC and cyclin D1 signaling in parental cells but significantly upregulated c-MYC and cyclin D1 signaling in AROE cells.

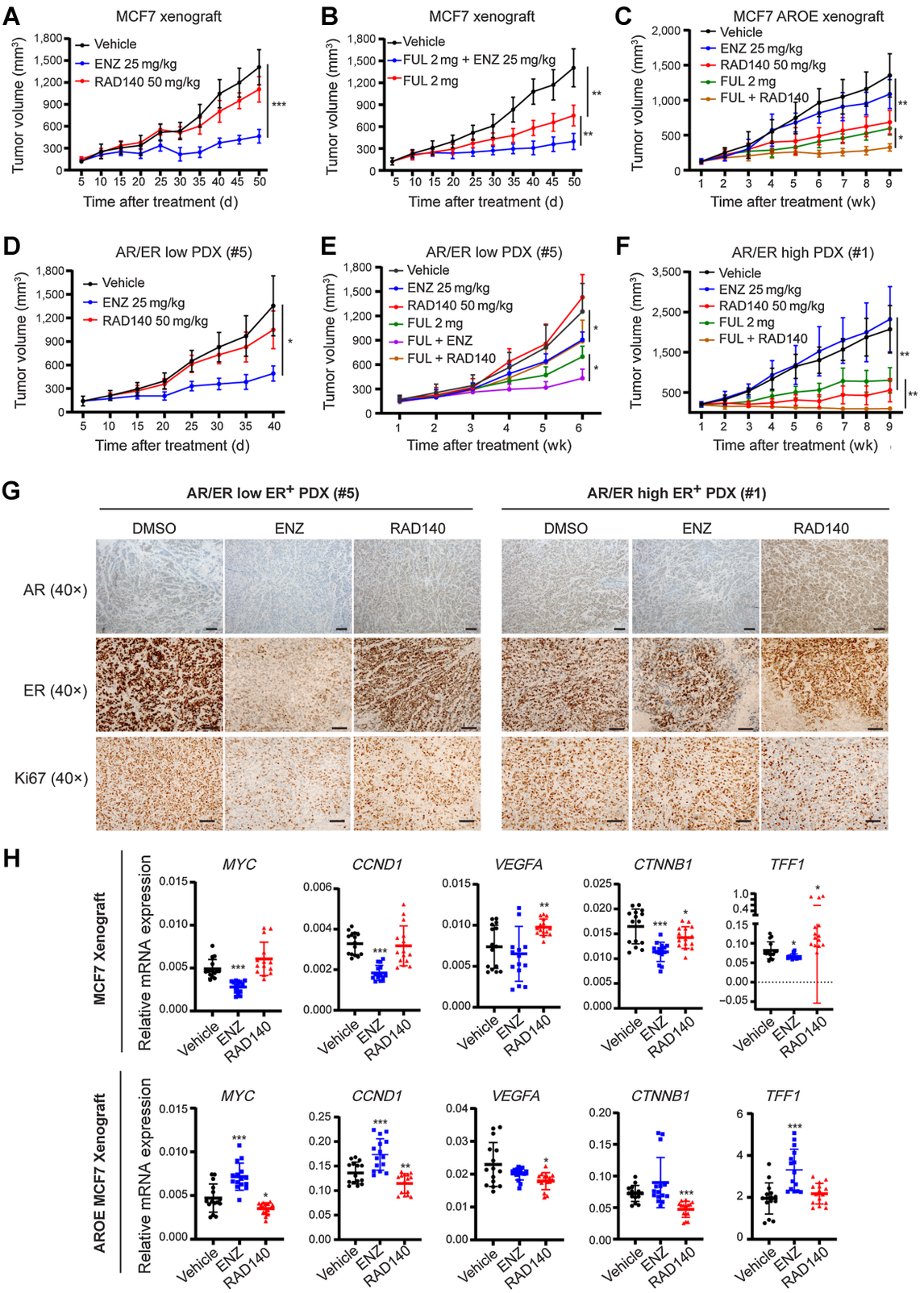
A
MCF7 xenograft
Vehicle
ENZ 25 mg/kg
RAD140 50 mg/kg
Tumor volume (mm3)
Time after treatment (d)
B
MCF7 xenograft
Vehicle
FUL 2 mg + ENZ 25 mg/kg
FUL 2 mg
Tumor volume (mm3)
Time after treatment (d)
C
MCF7 AROE xenograft
Vehicle
ENZ 25 mg/kg
RAD140 50 mg/kg
FUL 2 mg
FUL + RAD140
Tumor volume (mm3)
Time after treatment (wk)
D
AR/ER low PDX (#5)
Vehicle
ENZ 25 mg/kg
RAD140 50 mg/kg
Tumor volume (mm3)
Time after treatment (d)
E
AR/ER low PDX (#5)
Vehicle
ENZ 25 mg/kg
RAD140 50 mg/kg
FUL 2 mg
FUL + ENZ
FUL + RAD140
Tumor volume (mm3)
Time after treatment (wk)
F
AR/ER high PDX (#1)
Vehicle
ENZ 25 mg/kg
RAD140 50 mg/kg
FUL 2 mg
FUL + RAD140
Tumor volume (mm3)
Time after treatment (wk)
G
AR/ER low ER+ PDX (#5)
AR/ER high ER+ PDX (#1)
DMSO
ENZ
RAD140
AR (40×)
ER (40×)
Ki67 (40×)
H
MCF7 Xenograft
AROE MCF7 Xenograft
Relative mRNA expression
MYC
CCND1
VEGFA
CTNNB1
TFF1
Vehicle
ENZ
RAD140

has a unique structure that is distinct from other AR antagonists (36). The IC_{50} values of ENZ, RD162, apalutamide, and darolutamide in T47D cells were 8.64, 26.21, 18.38, and 5.66 μmol/L. RD162 and apalutamide had much lower inhibition efficiency than ENZ in breast cancer cells, and no significant difference was observed between AR-high and AR-low cells. Compared with ENZ, darolutamide was more effective in AR-low T47D cells than AR-high HCC1419 cells (Supplementary Fig. S3A). We measured the treatment effect of darolutamide in ARKO and ERKD cells. The results showed that the cell growth inhibition effect of darolutamide was not significantly altered in ARKO cells when compared with control but diminished dramatically in ERKD cells (Supplementary Fig. S3B and S3C). Those results indicated that darolutamide might have the same property as ENZ in treating AR-low ER$^+$ breast cancer. RD162 had a limited effect on MCF7 cell growth (Supplementary Fig. S3D). RD162 did not impair E2-induced ERE activity (Supplementary Fig. S3E), which might explain its low effectiveness in ER$^+$ cells. The mechanism underlying the different response and structure relationship with ER of those antiandrogens remains to be determined.

Enzalutamide recovered ER signaling through antagonizing AR in "AR-high" breast cancer cell lines

To illustrate the AR and ER genomic bindings after ENZ treatment in both MCF7 and MCF7 with AR overexpression (AROE) cells, we analyzed ChIP-seq data under four conditions, DMSO and ENZ treatment in parental and AROE MCF7 cells integratively. Compared with parental MCF7 cells, 11,189 AR-binding peaks were newly identified and 12,800 (60.05%) of ERα-binding peaks disappeared in AROE MCF7 cells (**Fig. 3A**). We overlapped the AROE-induced AR-binding peaks and AROE diminished ERα-binding peaks to determine whether AR was competing with ERα on genomic occupancy. Interestingly, only 14.48% (1,554/10,734) of ER-binding peaks were replaced by AR directly (**Fig. 3B**), which indicates that the direct competition of the genomic binding between AR and ERα explained no more than 15% of reduced ER peaks caused by AROE. Consistent with previous publications (37, 38), FOXA1 and FOXA2 motifs were highly enriched in AR gain and ER loss peaks (Supplementary Fig. S4A and S4B). AR and ER have similar genetic distribution profiles, with around 20% of peaks occurring at upstream promoter regions. A plurality of peaks occurred in distal intergenic regions (Supplementary Fig. S4C). Consistent with our functional studies, ER binding was dramatically decreased after ENZ treatment in MCF7 parental cells (**Fig. 3C**, DMSO vs. ENZ). Moreover, AROE significantly decreased ERα binding globally (**Fig. 3A** and **C**, DMSO in parental MCF7 vs. DMSO in AROE MCF7). Interestingly, ERα was much more enriched when AR binding was blocked by ENZ in AROE cells (DMSO vs. ENZ in AROE MCF7, **Fig. 3C**, ER bindings, and **Fig. 3D**, AR bindings). The inhibition effect of AR on ERα binding was neutralized by ENZ treatment (**Fig. 3C**). Our results showed a competing relationship between AR and ERα, supporting the tumor suppressor role of AR in ER$^+$ breast cancer.

To further study the difference of ENZ response genes in parental and AROE MCF7 cells, we first did pathway analysis of ENZ-regulated genes (FC > 1.5 or < 0.67, FDR < 0.05) in parental and AROE MCF7 cells. The results showed that estrogen response-early and -late gene sets were the most significant pathways in both parental and AROE MCF7 cells (**Fig. 3E**; Supplementary Table S4). We found that estrogen response pathways were enriched in the DMSO group in parental MCF7 cells and were enriched in ENZ group in AROE cells (Supplementary Fig. S5A). We generated a heatmap of all 283 estrogen response-early and -late genes (GSEA gene sets). After *k*-means clustering analysis ($K = 3$), we identified a group of genes substantially stimulated by ENZ in AROE cells, including *MYC, CCND1*, and *TFF1* (**Fig. 3F**; Supplementary Table S5). Meanwhile, androgen downstream response genes were inhibited more robustly in AROE cells than parental cells (Supplementary Fig. S5B). We observed downregulation of oncogenic signaling (*VEGFA, MYC, CCND1*, and *CTNNB1*) of ENZ in MCF7 cells and an upregulation of those oncogenic signaling in AROE MCF7 cells (**Fig. 3G**; Supplementary Fig. S5C; Supplementary Table S6). In HCC1419 and CAMA1 AR-high cells, ERα was slightly decreased after ENZ treatment (Supplementary Fig. S5D). However, the mRNA levels of ER downstream genes (*MYC, CCND1*, and *TFF1*), *VEGFA*, and *CTNNB1* were upregulated by ENZ (Supplementary Fig. S5E, bottom). On the other hand, all those 5 genes were decreased after ENZ treatment in MCF7 and T47D AR-low cells (Supplementary Fig. S5E, top). Examining the ChIP-seq data of those genes, we found that AR and ERα were co-occupied at promoter regions of *TFF1* and *CCND1* whereas AR binding was not detected around *MYC* and *VEGFA* (Supplementary Fig. S5F and S5G), suggesting that AR downregulated ERα downstream genes through both genomic (*TFF1* and *CCND1*) and non-genomic (*MYC* and *VEGFA*) effect. It was reported that *MYC, CCND1*, and *TFF1* were downregulated after RAD140 treatment in the AR$^+$ PDX model (30). In our study, ERα was downregulated by RAD140 only in HCC1419 and CAMA1 cells with relatively high AR expressed (Supplementary Fig. S6A). In summary, our data argue against the use of ENZ in patients with AR-high breast cancer and highlighted the importance of defining a more quantitative relationship between AR, ERα, and response to RAD140 or ENZ.

Quantitative correlation between AR/ER ratio and response to RAD140 or ENZ

On the basis of previous data, we hypothesized that the AR and ERα relationship determined the response of AR-targeting therapy in ER$^+$ breast cancers. We further explored the clinical application of AR and

Figure 5.

In vivo efficacy evaluation of RAD140 and ENZ in xenograft models with low and high AR/ER. **A–F,** The effect of RAD140, ENZ, and their combination with fulvestrant on the growth of AR-high and -low xenografts. A total of 25-mg/kg ENZ and 50-mg/kg RAD140 was administered orally 5 times per week. Fulvestrant was injected at 2 mg/wk subcutaneously. Tumor volumes were measured at the indicated times using vernier calipers: volume = length × width^2/2. Data points represent the mean ± SD tumor volume of each treatment group ($n = 5$). Comparisons were done between indicated groups at the ethical endpoint. *, $P < 0.05$; **, $P < 0.01$; ***, $P < 0.001$, unpaired two-tailed Student *t* test. **A,** Xenograft tumor growth of MCF7 control cells harbor empty vector PLVX3 (MCF7 xenograft) under RAD140 and ENZ treatment. **B,** MCF7 xenografts treated with vehicle, fulvestrant, and a combination of ENZ and fulvestrant. **C,** Xenograft tumor growth of MCF7 AROE cells harbors AR-PLVX3 (MCF7 AROE xenograft) under RAD140, ENZ, fulvestrant, and fulvestrant+RAD140 treatment. **D,** Growth curves of AR/ER-low ER$^+$ PDX following vehicle, ENZ, or RAD140 treatment. **E,** AR/ER-low xenografts treated with ENZ, RAD140, fulvestrant, fulvestrant+ENZ, and fulvestrant+RAD140. **F,** AR/ER-high xenograft tumor growth under RAD140, ENZ, fulvestrant, and fulvestrant+RAD140 treatment. Data are mean ± SD of 5 replicates for **A–D**. Data are mean ± SD of 4 to 5 replicates for **E**. Data are mean ± SD of 6 replicates for **F**. *, $P < 0.05$; **, $P < 0.01$; ***, $P < 0.001$, unpaired two-tailed Student *t* test for indicated comparison. **G,** IHC staining of AR, ER, and Ki67 in AR/ER-high and -low PDX tumor section under ENZ and RAD140 treatment. Magnification, ×40. Bar, 100 μm. **H,** qPCR validation of *MYC, CCND1, VEGFA, CTNNB1*, and *TFF1* in MCF7 and MCF7 AROE xenografts treated with ENZ and RAD140. Gene expression was normalized to the reference gene *GAPDH*. Data are presented as mean ± SD (5 mice × 3 replicates). *, $P < 0.05$; ***, $P < 0.001$, unpaired two-tailed Student *t* test for indicated comparison.

ERα in predicting ENZ and RAD140 response. We manipulated AR and ERα expression levels in MCF7 and T47D cells using a doxycycline-inducible expression system (**Fig. 4A**). We found that the AUC of RAD140 was negatively associated with AR protein levels ($P < 0.001$) and not significantly associated with ERα expression levels. On the other hand, the AUC of ENZ was significantly positively associated with AR expression ($P < 0.01$) but negatively associated with ERα protein ($P < 0.01$; **Fig. 4B** and **C**). Considering both AR and ERα in our model, we found that higher AR/ERα levels predicted a better response to RAD140 and a worse response to ENZ. Although on the contrary, lower AR/ERα levels were associated with a better response to ENZ but a worse response to RAD140 (**Fig. 4D**). We further checked the relative AR to ER level in ER^+ breast cancer cell lines. We found that MCF7 and T47D have lower AR to ER ratios than HCC1419 and CAMA1in both mRNA and protein levels (Supplementary Fig. S6B and S6C), which explained the differential response to ENZ and RAD140 we identified previously.

In vivo differential response to AR agonist RAD140 and AR antagonist ENZ

To assess *in vivo* efficacy of ENZ and RAD140 in ER^+ breast cancers, MCF7 cells stably transfected with vector control PLVX3 or AR-PLVX3 plasmid were used to create MCF7 and MCF7 AROE xenografts (**Fig. 1I**, control vs. #3). In the MCF7 xenografts transfected with vector control (AR<ERα), five mice treated with ENZ showed significant tumor regression by the end of the treatment schedule (**Fig. 5A**; Supplementary Fig. S7A). RAD140 did not affect tumor growth compared with vehicle control, demonstrating that ENZ had better efficacy in control xenografts with low AR/ERα. Importantly, ENZ statistically increased the tumor inhibition effects of fulvestrant in AR/ERα-low MCF7 xenograft tumors (**Fig. 5B**; Supplementary Fig. S7B). In contrast, oral administration of RAD140 induced significant tumor growth inhibition of 56.11% in AROE xenograft models (AR > ERα), showing the same efficacy as fulvestrant (**Fig. 5C**; Supplementary Fig. S7C). Significant improvement in tumor growth inhibition was observed in mice treated with combined RAD140 and fulvestrant when compared with fulvestrant alone (**Fig. 5C**; Supplementary Fig. S7C). No weight loss was detected in combination drug group (Supplementary Fig. S7A–S7C). These findings corroborated our previous *in vitro* results, demonstrating that RAD140 and ENZ showed differential tumor regression efficiency in control MCF7 xenografts (low AR/ER) vs. AROE MCF7 xenografts (high AR/ER).

Two ER^+ PDXs selected on the basis of AR/ER (high and low ratios) were used to test the response of ENZ and RAD140. We scanned the expression of AR and ER in our ER^+ PDX models (39, 40). An extremely low AR/ER ratio model (#5, Supplementary Fig. S8A) and an extremely high AR/ER ratio model (#1, Supplementary Fig. S8A) were treated with ENZ and RAD140. After 6 weeks of treatment, in AR/ER-low xenograft models (#5), the ENZ treatment group had markedly reduced tumor volume compared with the RAD140 treatment and vehicle groups. No inhibition effect was observed under RAD140 treatment (**Fig. 5D**; Supplementary Fig. S8B). Combined with fulvestrant, ENZ showed a better tumor depression effect than fulvestrant alone (**Fig. 5E**; Supplementary Fig. S8C). In AR/ER-high tumors, by week 9 of the study, the RAD140 treatment groups exhibited a 73.27% reduction in tumor volume relative to the vehicle treatment group (**Fig. 5F**; Supplementary Fig. S8D). The combination of RAD140 and fulvestrant treatment was much more effective than either monotherapy and did not cause any significant animal weight loss (**Fig. 5F**; Supplementary Fig. S8D). These results indicate that ENZ has better efficacy in treating ER-dominant (AR < ER) tumor and RAD140 are more effective in AR-dominant (AR > ER) tumor.

To confirm the effective genes of ENZ and RAD140, we measured the AR, ERα, and Ki67 protein levels and mRNA levels of downstream genes in tumors harvested at the endpoint. In the MCF7 or AR-low PDX (#5) model, ENZ reduced the expression of AR, ERα, and the proliferation marker Ki67 relative to the control group. RAD140 slightly induced AR expression but had no effect on ERα and Ki67 expressions (**Fig. 5G**; Supplementary Fig. S8E). On the contrary, in the AR-high xenograft model, RAD140 decreased Ki67 expression without AR or ERα reduction (**Fig. 5G**; Supplementary Fig. S8E). Furthermore, ER downstream genes (*MYC, CCND1, CTNNB1*, and *TFF1*) were reduced by ENZ in MCF7 xenograft tumors. However, in AROE xenografts, *MYC* and *CCND1* were greatly stimulated by ENZ. On the other hand, AROE tumors under RAD140 treatment had a significant reduction of ER-regulated genes (**Fig. 5H**). A previous study reported that RAD140 inhibited cancer growth by repressing ERα expression (30). We observed ERα decrease after RAD140 treatment in HCC1419 and CAMA1 cells (AR > ER; Supplementary Fig. S6A). However, in the MCF7 AROE xenograft model (AR > ER) the ER downstream genes were downregulated although ERα level was little changed under RAD140 treatment (**Fig. 5G** and **H**). Another study found that AR activation repressed ER-regulated cell-cycle genes by altering the genomic distribution of ERα and essential co-activators (23). In general, our data showed that, *in vivo*, RAD140 exhibited strong antitumor activity via AR-dependent ERα inactivation.

The AR/ER ratio in primary and metastatic breast cancers: implications for individualized AR-targeted therapy

AR is coexpressed with ER in ER^+ breast cancer (10, 41). To explore the distribution of AR/ER, we quantified AR and ERα protein levels in a TMA consisting of 68 ER^+ breast cancers. 61.76% were AR-positive tumors and the expression of AR was positively correlated with ER ($r = 0.28$, $P_{spearman} = 0.02$). On the basis of the staining intensity, two subgroups of individuals have $AR3^+/ER^+$ or $AR^-/ER3^+$ immunophenotype in the proportion of 2.94% and 14.71%, respectively (**Fig. 6A**). The representative images were shown in Supplementary Fig. S9A. The IHC score (percentage × intensity) was used to further quantify the expression of AR and ERα. The distribution of the relative AR to ERα levels (AR/ER) is shown in **Fig. 6**B. We found that 88.24% cases were ER dominant tumors (AR/ER<1) and 11.76% cases were AR dominant tumors (AR/ER>1; **Fig. 6B**). In the TCGA cohort, the incidence of AR dominant tumors was 15.85% (TCGA, Firehose Legacy, Reverse Phase Protein Array, $N = 347$, **Fig. 6C**). Determination of AR/ER status may provide additional information and guide the endocrine drug selection for patients with ER^+ breast cancer.

We compared the AR, ER level, and AR/ER ratio in primary and metastatic breast cancer. *AR* and *ESR1* mRNA expression of 140 metastatic samples and 235 primary samples were used in the analysis (GSE124648; ref. 42). We found that AR/ER ratios were significantly higher in metastatic breast cancer than primary breast cancer ($P < 0.001$, **Fig. 6D**). *ESR1* levels were lower in patients with metastatic breast cancer than in primary breast cancer ($P = 0.012$), whereas *AR* levels were not significantly different (Supplementary Fig. S9B and S9C). Moreover, we performed survival analysis using this metastatic breast cancer cohort. We included 97 patients treated with endocrine therapy after their metastatic recurrence in the analysis. Women with low AR/ER ratio tumors had a longer PFS and OS than women with AR/ER-high tumors ($P = 0.005$, PFS; $P = 0.040$, OS; **Fig. 6E**

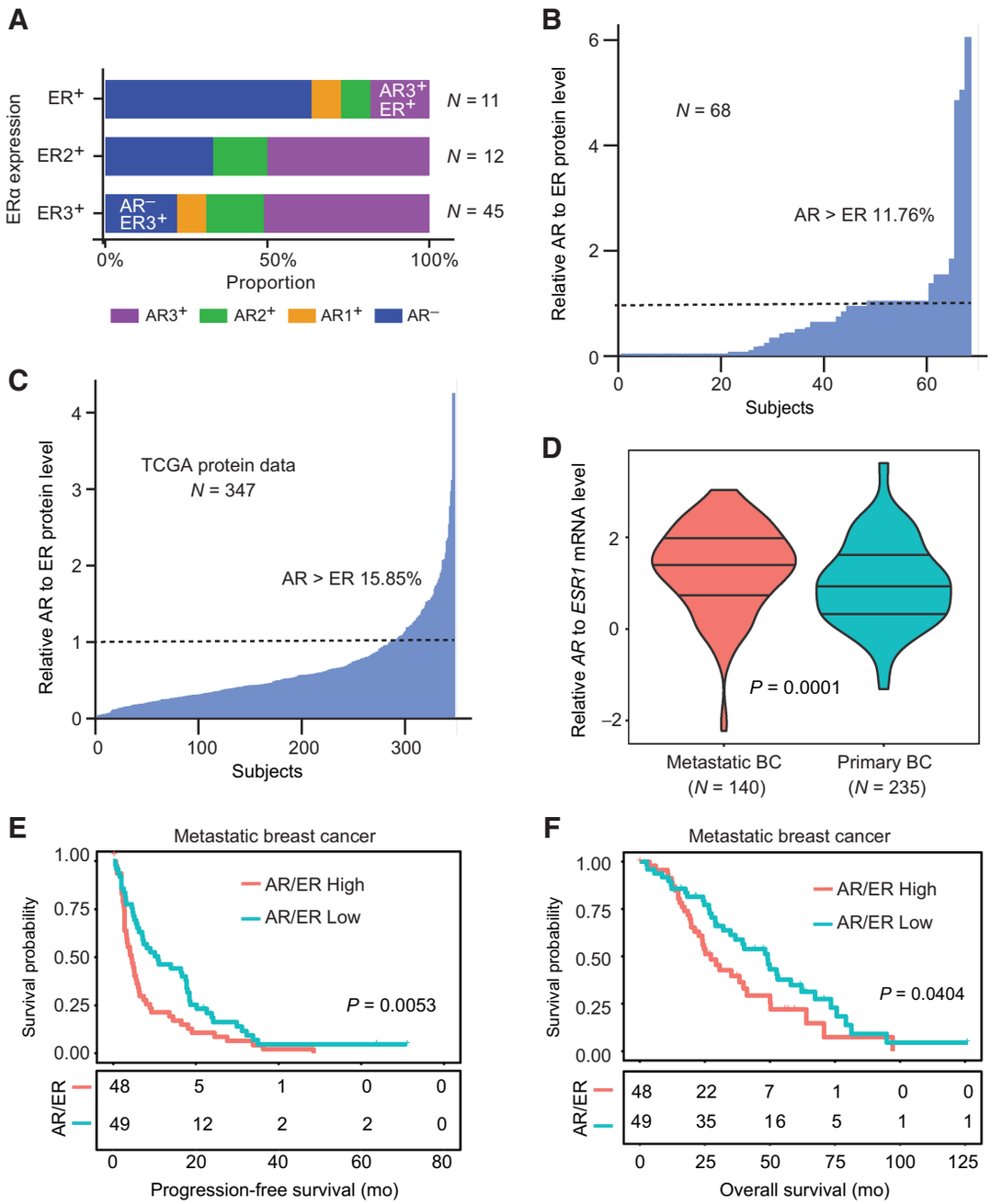

Figure 6.

Relative AR/ER expression in primary and metastatic ER$^+$ breast cancers. **A,** Bar chart of the percentage of AR staining intensity in ER weak (+), intermediate (2+), and strong (3+) tumors in IHC cohort. The intensity of nuclei immunoreactivity was assessed semiquantitatively on a scale of 0 to 3 (none, weak, intermediate, and strong). **B,** Distribution of AR/ER in IHC cohort ($n = 68$). Expressions were quantified using IHC scores, positive cell percentage × intensity. **C,** Distribution of AR/ER in TCGA breast cancer cohort ($n = 347$). The reverse phase protein array was used to test AR and ER protein levels. **D,** Violin plot of AR/ER level in primary and metastatic breast cancer. Bars are presented as 25th percentile (bottom quartile), median, and 75th percentile (top quartile). AR/ER is higher in metastatic cancer than in primary cancer (primary vs. metastatic, median 0.047 vs. 0.689, unpaired two-tailed Student *t* test, $P = 0.0001$). **E** and **F,** Kaplan–Meier survival curves displaying the estimated survival probability for two different groups (AR/ER high vs. low) of metastatic breast cancer. Patients with metastatic breast cancer ($n = 97$) subsequently treated with endocrine therapy were included in the analysis. Patients with AR/ER-high or -low groups were separated by median of AR/ER level in the cohort. The number of events (total deaths in each group) is indicated. Patients with lower AR/ER levels have a more favorable prognosis compared with patients who have higher AR/ER levels. **E,** Progression-free survival. **F,** Overall survival. The log-rank test indicates a significant difference between the survival curves.

and **F**), suggesting that high AR/ER ratio tumors were associated with resistance to endocrine therapy and predicted a worse prognosis in women with metastatic breast cancer. In addition, we noted a longer PFS in women with ESR1-high tumors compared with those with ESR1-low tumors ($P = 0.022$, Supplementary Fig. S9D). However, no significant association was found between AR level and PFS or OS (Supplementary Fig. S9E). In general, AR/ER ratio is upregulated in metastatic breast cancer and associated with worse clinical outcomes in metastatic breast cancer. These data indicate the importance of AR/ER quantification in metastatic breast cancer and highlight the application of AR agonists in treating metastatic breast cancer.

Discussion

In this study, we demonstrated that the responses of AR-targeting drugs were associated with both AR and ERα status, providing insights into the controversies regarding the roles of AR and AR-targeting drugs in ER^+ breast cancer. We found that ER signaling was repressed by AR overexpression through genetic and non-genetic competition. Our results support the tumor suppressor role of AR in ER^+ breast cancer, consistent with the published clinical and biological data (11, 23). One important result of our study was the dynamic efficacies and outcomes of AR agonist and antagonist in the presence of different AR and ERα levels. In AR-low or ERα-dominant breast cancer cells, ENZ inhibits cell proliferation effectively by antagonizing ERα, which is not dependent on AR. RAD140 has no effect because of insufficient target AR expressed. By contrast, in AR-high cells, RAD140 activates AR signaling and suppressed tumor growth by deregulating ERα expression and blocking ERα downstream genes, whereas ENZ leads to recovery of the repression of AR on ERα transcription thus stimulating cell growth.

Several possible reasons have been proposed to explain the divergent viewpoints of AR function in ER^+ breast cancer, including the ratio of AR to ERα (28) and the background of ER/PR/HER2 expression (43). The clinical significance of AR to ERα ratios has been studied recently. It was reported that a subgroup of patients with AR/ERα ratio ≥2 had a worse breast cancer prognosis with aggressive biological features than tumors with ratios of AR/ERα < 2 (44, 45). Patients with a high AR/ERα ratio in primary tumors had better prognoses in terms of OS (46). Our data suggest that joint evaluation of AR and ER expression may identify two subsets of tumors with implications regarding the choice of an AR agonist or AR antagonist. RAD140 has better inhibition effect in AR-dominant tumors (AR > ER) whereas ENZ is more efficacious in ER-dominant tumors (AR < ER). Our results predict the drug preference in ER^+ tumors with extremely high or low AR/ER and provide the basis for the conduct of prospective clinical trials.

Another interesting finding of our study is the opposite effects of ENZ in AR/ER-low and AR/ER-high ER^+ breast cancer. The amounts of AR and ER protein and their binding affinities to ENZ co-determine the targeting priority of ENZ. Similar to our finding that ENZ effects in MCF7 cells are not dependent on AR level, ENZ could not recapitulate the effect of AR KD in MCF7 cells and had no effect in endocrine-resistant PDX models (29). Our study is the first to identify the tumor promotion effect of ENZ in AR-high cells, which raises concern regarding the use of ENZ in AR-high ER^+ breast cancer. We observed direct binding of ENZ and full-length ERα in our radiolabeled assay; however, the exact ENZ-ERα-binding pocket is still unknown. ENZ cannot fully compete E2, indicating a possibility that ENZ might be an allosteric inhibitor. RD162, another AR antagonist, has no binding to full-length ERα under 0.1 mmol/L (34). The efficiency of ENZ and RD162 differs, although they have similar chemical structures. Darolutamide could inhibit cell growth as effectively as ENZ, whereas their structures are distinct from each other. The structural relationship between ERα and those AR antagonists, as well as the conformational change induced by the interaction, is still unclear and will require further studies. Our results provide insights into the clinical application of AR agonists in ER^+ breast cancer and support the use of an AR agonist in AR/ER-high ER^+ cancers. Our data suggest that the AR/ER ratio might be a marker upon which to base the selection of an AR agonist or an AR antagonist for therapy.

The limitations of our study are the relatively small number of cell lines and mice models studied and the preliminary methodology for biomarker quantification. The assessment of the AR/ER ratio in our models was exploratory and was based mainly on Western blot analysis, which is not likely a choice of the assay for clinical application. A previous study that was designed to examine the combined effect of ENZ and exemestane in treating patients with advanced/metastatic breast cancer found that receiving ENZ treatment with both high *AR* levels and low *ESR1* levels had a greatly improved PFS compared with the control group (15). However, they used the median cutoff point to define the high and low expressions. In our cell-line–inducible models, we observed a quantitative relationship between AR/ER and response to RAD140 or ENZ response. We also observed that the ENZ and fulvestrant combination was more effective than fulvestrant alone in ER-high and AR-low primary breast cancer animal models. The dynamic ranges of hormone receptor status in cancer development and approaches used to define high or low expression might partially explain this discrepancy. Further studies in larger clinical cohorts are required to build quantitative models with dynamic AR/ER ratios to assess the association with drug response.

Authors' Disclosures

J.M. Carter reports personal fees from Astra Zeneca outside the submitted work. J.C. Boughey reports grants from Eli Lilly outside the submitted work. M.P. Goetz reports other support from ARC Therapeutics, AstraZeneca, Biotheranostics, Blueprint Medicines, Lilly, RNA Diagnostics, Sanofi Genzyme, and Seattle Genetics, grants from Lilly, Pfizer, and Sermonix, and personal fees from Research to Practice, Clinical Education Alliance, Medscape, MJH Life Sciences, Curio Science, and Total Health Conferencing outside the submitted work. R.M. Weinshilboum reports being a co-founder and a stockholder in OneOme, a Pharmacogenomic decision-support company. J.N. Ingle reports grants from The Breast Cancer Research Foundation, National Cancer Institute, the George M. Eisenberg Foundation for Charities, and Regis Foundation during the conduct of the study. No disclosures were reported by the other authors.

Authors' Contributions

L. Wei: Data curation, formal analysis, validation, investigation, writing–original draft. **H. Gao:** Data curation, software, formal analysis, visualization. **J. Yu:** Resources, methodology. **H. Zhang:** Data curation, methodology. **T.T.L. Nguyen:** Software, formal analysis, visualization. **Y. Gu:** Data curation, methodology. **M.R. Passow:** Data curation, methodology. **J.M. Carter:** Data curation, formal analysis, methodology. **B. Qin:** Resources. **J.C. Boughey:** Resources. **M.P. Goetz:** Resources. **R.M. Weinshilboum:** Supervision. **J.N. Ingle:** Conceptualization, funding acquisition, writing–review and editing. **L. Wang:** Conceptualization, supervision, funding acquisition, project administration, writing–review and editing.

Acknowledgments

This work was supported by the Breast Cancer Research Foundation (BCRF-20–076), the Mayo Clinic Breast Cancer Specialized Program of Research Excellence Grant (P50CA 116201), the Mayo Clinic Cancer Center Support Grant (P30

CA15083), the George M. Eisenberg Foundation for Charities, and the Regis Foundation.

The publication costs of this article were defrayed in part by the payment of publication fees. Therefore, and solely to indicate this fact, this article is hereby marked "advertisement" in accordance with 18 USC section 1734.

Note

Supplementary data for this article are available at Cancer Research Online (http://cancerres.aacrjournals.org/).

Received March 24, 2022; revised October 4, 2022; accepted November 30, 2022; published first December 5, 2022.

References

1. Sung H, Ferlay J, Siegel RL, Laversanne M, Soerjomataram I, Jemal A, et al. Global Cancer Statistics 2020: GLOBOCAN estimates of incidence and mortality worldwide for 36 cancers in 185 countries. CA Cancer J Clin 2021;71:209–49.
2. Heer E, Harper A, Escandor N, Sung H, McCormack V, Fidler-Benaoudia MM. Global burden and trends in premenopausal and postmenopausal breast cancer: a population-based study. The Lancet Global Health 2020;8:e1027–e37.
3. Siegel RL, Miller KD, Fuchs HE, Jemal A. Cancer statistics, 2022. CA Cancer J Clin 2022;72:7–33.
4. Collins LC, Cole KS, Marotti JD, Hu R, Schnitt SJ, Tamimi RM. Androgen receptor expression in breast cancer in relation to molecular phenotype: results from the Nurses' Health Study. Mod Pathol 2011;24:924–31.
5. Vera-Badillo FE, Templeton AJ, de Gouveia P, Diaz-Padilla I, Bedard PL, Al-Mubarak M, et al. Androgen receptor expression and outcomes in early breast cancer: a systematic review and meta-analysis. J Natl Cancer Inst 2014;106: djt319.
6. Rugo HS, Rumble RB, Macrae E, Barton DL, Connolly HK, Dickler MN, et al. Endocrine therapy for hormone receptor-positive metastatic breast cancer: American Society of Clinical Oncology Guideline. J Clin Oncol 2016;34: 3069–103.
7. Lin NU, Winer EP. Advances in adjuvant endocrine therapy for postmenopausal women. J Clin Oncol 2008;26:798–805.
8. Pan H, Gray R, Braybrooke J, Davies C, Taylor C, McGale P, et al. 20-year risks of breast-cancer recurrence after stopping endocrine therapy at 5 years. N Engl J Med 2017;377:1836–46.
9. Hu R, Dawood S, Holmes MD, Collins LC, Schnitt SJ, Cole K, et al. Androgen receptor expression and breast cancer survival in postmenopausal women. Clin Cancer Res 2011;17:1867–74.
10. Kensler KH, Poole EM, Heng YJ, Collins LC, Glass B, Beck AH, et al. Androgen receptor expression and breast cancer survival: results from the Nurses' Health Studies. J Natl Cancer Inst 2018;111:700–8.
11. Bozovic-Spasojevic I, Zardavas D, Brohee S, Ameye L, Fumagalli D, Ades F, et al. The prognostic role of androgen receptor in patients with early-stage breast cancer: a meta-analysis of clinical and gene expression data. Clin Cancer Res 2017;23:2702–12.
12. Birrell SN, Bentel JM, Hickey TE, Ricciardelli C, Weger MA, Horsfall DJ, et al. Androgens induce divergent proliferative responses in human breast cancer cell lines. J Steroid Biochem Mol Biol 1995;52:459–67.
13. Lin H-Y, Sun M, Lin C, Tang H-Y, London D, Shih A, et al. Androgen-induced human breast cancer cell proliferation is mediated by discrete mechanisms in estrogen receptor-α–positive and -negative breast cancer cells. J Steroid Biochem Mol Biol 2009;113:182–8.
14. Feng J, Li L, Zhang N, Liu J, Zhang L, Gao H, et al. Androgen and AR contribute to breast cancer development and metastasis: an insight of mechanisms. Oncogene 2017;36:2775–90.
15. Krop I, Abramson V, Colleoni M, Traina T, Holmes F, Garcia-Estevez L, et al. A randomized placebo controlled phase II trial evaluating exemestane with or without enzalutamide in patients with hormone receptor–positive breast cancer. Clin Cancer Res 2020;26:6149–57.
16. Zhao L, Han X, Lu J, McEachern D, Wang S. A highly potent PROTAC androgen receptor (AR) degrader ARD-61 effectively inhibits AR-positive breast cancer cell growth *in vitro* and tumor growth *in vivo*. Neoplasia 2020; 22:522–32.
17. Garay JP, Park BH. Androgen receptor as a targeted therapy for breast cancer. Am J Cancer Res 2012;2:434–45.
18. Kennedy BJ. Fluoxymesterone therapy in advanced breast cancer. N Engl J Med 1958;259:673–5.
19. Goldenberg IS. Testosterone propionate therapy in breast cancer. JAMA 1964; 188:1069–72.
20. Panet-Raymond V, Gottlieb B, Beitel LK, Pinsky L, Trifiro MA. Interactions between androgen and estrogen receptors and the effects on their transactivational properties. Mol Cell Endocrinol 2000;167: 139–50.
21. Lanzino M, De Amicis F, McPhaul MJ, Marsico S, Panno ML, Andò S. Endogenous coactivator ARA70 interacts with estrogen receptor alpha (ERalpha) and modulates the functional ERalpha/androgen receptor interplay in MCF-7 cells. J Biol Chem 2005;280:20421–30.
22. Casaburi I, Cesario MG, Donà A, Rizza P, Aquila S, Avena P, et al. Androgens downregulate miR-21 expression in breast cancer cells underlining the protective role of androgen receptor. Oncotarget 2016;7:12651–61.
23. Hickey TE, Selth LA, Chia KM, Laven-Law G, Milioli HH, Roden D, et al. The androgen receptor is a tumor suppressor in estrogen receptor–positive breast cancer. Nat Med 2021;27:310–20.
24. Aceto N, Bardia A, Wittner BS, Donaldson MC, O'Keefe R, Engstrom A, et al. AR expression in breast cancer CTCs associates with bone metastases. Mol Cancer Res 2018;16:720–7.
25. De Amicis F, Thirugnansampanthan J, Cui Y, Selever J, Beyer A, Parra I, et al. Androgen receptor overexpression induces tamoxifen resistance in human breast cancer cells. Breast Cancer Res Treat 2010;121:1–11.
26. Rechoum Y, Rovito D, Iacopetta D, Barone I, Andò S, Weigel NL, et al. AR collaborates with ERα in aromatase inhibitor-resistant breast cancer. Breast Cancer Res Treat 2014;147:473–85.
27. D'Amato NC, Gordon MA, Babbs B, Spoelstra NS, Carson Butterfield KT, Torkko KC, et al. Cooperative dynamics of AR and ER activity in breast cancer. Mol Cancer Res 2016;14:1054–67.
28. Cochrane DR, Bernales S, Jacobsen BM, Cittelly DM, Howe EN, D'Amato NC, et al. Role of the androgen receptor in breast cancer and preclinical analysis of enzalutamide. Breast Cancer Res 2014;16:R7.
29. Chia K, Milioli H, Portman N, Laven-Law G, Coulson R, Yong A, et al. Non-canonical AR activity facilitates endocrine resistance in breast cancer. Endocr Relat Cancer 2019;26:251–64.
30. Yu Z, He S, Wang D, Patel HK, Miller CP, Brown JL, et al. Selective androgen receptor modulator RAD140 inhibits the growth of androgen/estrogen receptor–positive breast cancer models with a distinct mechanism of action. Clin Cancer Res 2017;23:7608–20.
31. Gu G, Tian L, Herzog SK, Rechoum Y, Gelsomino L, Gao M, et al. Hormonal modulation of ESR1 mutant metastasis. Oncogene 2021;40: 997–1011.
32. Krämer A, Green J, Pollard J Jr, Tugendreich S. Causal analysis approaches in Ingenuity Pathway Analysis. Bioinformatics 2013;30:523–30.
33. Swerdloff RS, Dudley RE, Page ST, Wang C, Salameh WA. Dihydrotestosterone: biochemistry, physiology, and clinical implications of elevated blood levels. Endocr Rev 2017;38:220–54.
34. Tran C, Ouk S, Clegg NJ, Chen Y, Watson PA, Arora V, et al. Development of a second-generation antiandrogen for treatment of advanced prostate cancer. Science 2009;324:787–90.
35. Clegg NJ, Wongvipat J, Joseph JD, Tran C, Ouk S, Dilhas A, et al. ARN-509: a novel antiandrogen for prostate cancer treatment. Cancer Res 2012; 72:1494–503.
36. Fizazi K, Shore N, Tammela TL, Ulys A, Vjaters E, Polyakov S, et al. Darolutamide in nonmetastatic, castration-resistant prostate cancer. N Engl J Med 2019;380:1235–46.
37. Hurtado A, Holmes KA, Ross-Innes CS, Schmidt D, Carroll JS. FOXA1 is a key determinant of estrogen receptor function and endocrine response. Nat Genet 2011;43:27–33.
38. Robinson JL, Macarthur S, Ross-Innes CS, Tilley WD, Neal DE, Mills IG, et al. Androgen receptor driven transcription in molecular apocrine breast cancer is mediated by FoxA1. EMBO J 2011;30:3019–27.

39. Goetz MP, Kalari KR, Suman VJ, Moyer AM, Yu J, Visscher DW, et al. Tumor sequencing and patient-derived xenografts in the neoadjuvant treatment of breast cancer. J Natl Cancer Inst 2017;109:djw306.
40. Yu J, Qin B, Moyer AM, Sinnwell JP, Thompson KJ, Copland JA III, et al. Establishing and characterizing patient-derived xenografts using pre-chemotherapy percutaneous biopsy and post-chemotherapy surgical samples from a prospective neoadjuvant breast cancer study. Breast Cancer Res 2017; 19:130.
41. Vidula N, Yau C, Wolf D, Rugo HS. Androgen receptor gene expression in primary breast cancer. npj Breast Cancer 2019;5:47.
42. Sinn BV, Fu C, Lau R, Litton J, Tsai TH, Murthy R, et al. SETER/PR: a robust 18-gene predictor for sensitivity to endocrine therapy for metastatic breast cancer. NPJ Breast Cancer 2019;5:16.
43. Ni M, Chen Y, Fei T, Li D, Lim E, Liu XS, et al. Amplitude modulation of androgen signaling by c-MYC. Genes Dev 2013;27:734–48.
44. Rangel N, Rondon-Lagos M, Annaratone L, Aristizábal-Pachon AF, Cassoni P, Sapino A, et al. AR/ER ratio correlates with expression of proliferation markers and with distinct subset of breast tumors. Cells 2020;9:1064.
45. Rangel N, Rondon-Lagos M, Annaratone L, Osella-Abate S, Metovic J, Mano MP, et al. The role of the AR/ER ratio in ER-positive breast cancer patients. Endocr Relat Cancer 2018;25:163–72.
46. Bronte G, Rocca A, Ravaioli S, Scarpi E, Bonafè M, Puccetti M, et al. Evaluation of androgen receptor in relation to estrogen receptor (AR/ER) and progesterone receptor (AR/PgR): a new must in breast cancer? J Oncol 2019;2019:1393505.